Experiments in Fluids (2006) 40: 928–941
DOI 10.1007/s00348-006-0129-6

RESEARCH ARTICLE

A. S. Banerjee · A. C. Mandal · J. Dey

Particle image velocimetry studies of an incipient spot in the Blasius boundary layer

Received: 9 August 2005 / Revised: 23 December 2005 / Accepted: 2 February 2006 / Published online: 10 March 2006

Abstract Spatial evolution of a small amplitude localized disturbance introduced into the laminar boundary layer of a flat plate has been studied experimentally using the particle image velocimetry (PIV) technique. PIV data have been acquired in the spanwise and wall normal planes. Long and well defined high and low speed streaks are seen in the spanwise plane. The number of streaks are found to increase in the downstream direction. Breathing mode type oscillation of the boundary layer is observed. Associated with the streaks and akin to the bypass transition, 'backward' and 'forward' jet like structures of the fluctuating velocity components are observed.

1 Introduction

In order to understand the breakdown of a laminar boundary layer, many investigations have been carried out in the past with artificial disturbances introduced into the boundary layer. Gaster and Grant (1975) have studied the evolution of small amplitude disturbance in a laminar boundary layer and observed growing wave packets. Artificial turbulent spots, which are created by large amplitude disturbances, have been studied by many investigators (e. g., Schubauer and Klebanoff 1955; Wygnanski et al. 1982; Gutmark and Blackwelder 1987, to name a few). Amini and Lespinard (1982) have studied the propagation characteristics of an incipient spot in a constant pressure boundary layer. The disturbance studied by these authors lay somewhere in between those causing the formation of wave packets and turbulent spots, so as to enable them to study the disturbance preceding the turbulent spot. The characteristics of an incipient spot studied by Amini and Lespinard (1982) are: the maximum amplitude of the disturbance occurs away from the wall, and the spanwise envelope of the propagating disturbance is contained within an apex angle of $\approx 10°$, compared to the $\sim 22°$ apex angle of turbulent spots (Wygnanski et al. 1982). Breuer and Haritonidis (1990) have studied the evolution of small amplitude disturbance in a laminar boundary layer. These authors show that a small amplitude disturbance contains a dispersive and transient component. Their measurements, which agree qualitatively with their inviscid theory, show a rapid formation of induced shear layer in the boundary layer. Downstream the transient component of the disturbance decays owing to the viscous effect, but the linearly unstable dispersive part makes a dispersive wave packet. Westin et al. (1998) have studied the propagation of a localized disturbance introduced upstream of the flat plate leading edge. The disturbance so introduced is found by them to produce streaks in the downstream direction. Boiko et al. (2002) pointed out that the main feature during the development of a disturbance generated at the wall is similar due to the disturbance introduced in the freestream. In the case of freestream induced transition, the presence of the spanwise streaks is well established by the recent experimental study of Matsubara and Alfredsson (2001) and the DNS results of Jacobs and Durbin (2001). Compared to the available literature on turbulent spots, the studies on incipient spots are scarce, although successive incipient spots also cause flow breakdown; in fact, more work is needed in this regard, as pointed out by Amini and Lespinard (1982). In this paper we report the results of our study made using the particle image velocimetry (PIV) technique on the propagation of an incipient spot in a constant pressure boundary layer. Schröder and Kompenhans (2004) have studied the details of mixing and sub-structures in a turbulent spot using the multi-plane stereo particle image velocimetry technique, which has made it possible to make such detail studies.

AS Banerjee: summer trainee, IIT Kharagpur, India

A. S. Banerjee · A. C. Mandal · J. Dey (✉)
Department of Aerospace Engineering, Indian Institute of Science, Bangalore, 560012, India
E-mail: jd@aero.iisc.ernet.in

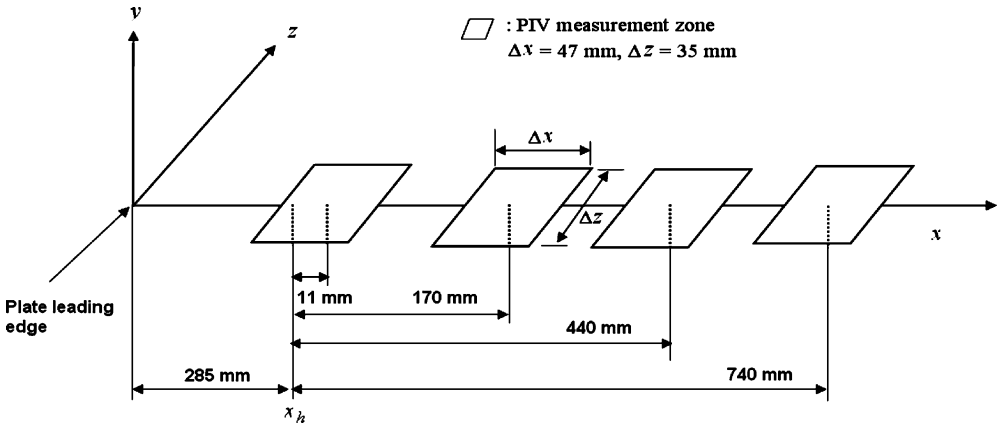

Fig. 1 Measurement stations and PIV measurement region. x_h: Disturbance source. Measurement stations: $x - x_h = 11$, 170, 440, and 740 mm

2 Experimental details

The experiments were carried out in the low turbulence wind tunnel available at the Department of Aerospace Engineering. Briefly, this was an open circuit tunnel with a square test section of dimensions 500×500×3,000 mm; a sketch of the tunnel is available in Vasudevan et al. (2001). The settling chamber ahead of the contraction had a smooth entry section with honeycomb and screens (four screens; 8 mesh/cm). The contraction ratio was 14:1, and its shape ensured a monotonic velocity increase. The tunnel had a short diffuser which was isolated from the rest of the tunnel by a flexible rubber band to minimize the transmission of vibrations to the test section. The tunnel speed was controlled by a speed controller that regulated a 5 kW DC motor, which drove the fan at the diffuser end.

The measurements in a constant pressure boundary layer were made on a flat plate that was placed horizontally in the mid-plane of the test section. The plate leading edge was of super-ellipse shape (Narasimha and Prasad 1994), which merged smoothly with the plate; this shape had been used in many earlier constant pressure experiments (Narasimha et al. 1984; Vasudevan et al. 2001). Since the plate was made of aluminium, the reflection of the laser sheet from the plate was not desirable as it contaminated the measurements. A smooth black sticker of 0.1 mm thickness was wrapped around the entire flat plate to reduce the reflection of the laser sheet from the plate surface. Both the hot-wire and the PIV measurements reported here were made on this smooth black surface stuck to the flat plate. As shown in Fig. 1, the streamwise, the wall normal, and the spanwise distances are denoted by x, y, and z, respectively; $x = 0$ corresponds to the flat plate leading edge. Δx and Δz in this figure denotes the streamwise and spanwise distances of the PIV measurement regions. At $x_h = 285$ mm from the plate leading edge and in the central plane ($z = 0$), a loudspeaker driven disturbance was introduced through a 1 mm hole on the plate. The downstream evolution of this disturbance was measured at $x - x_h = 11$, 170, 440,

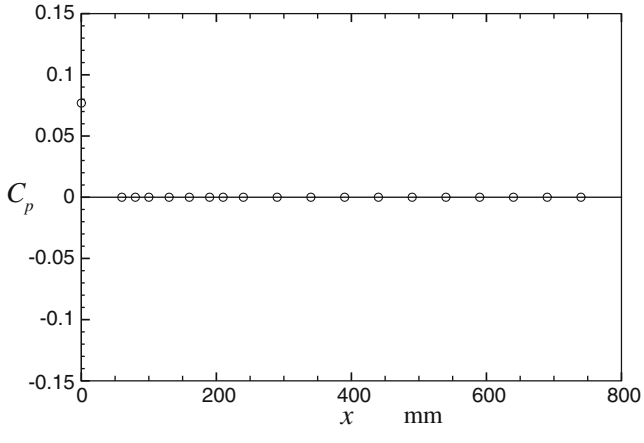

Fig. 2 Streamwise pressure distribution in the tunnel test section

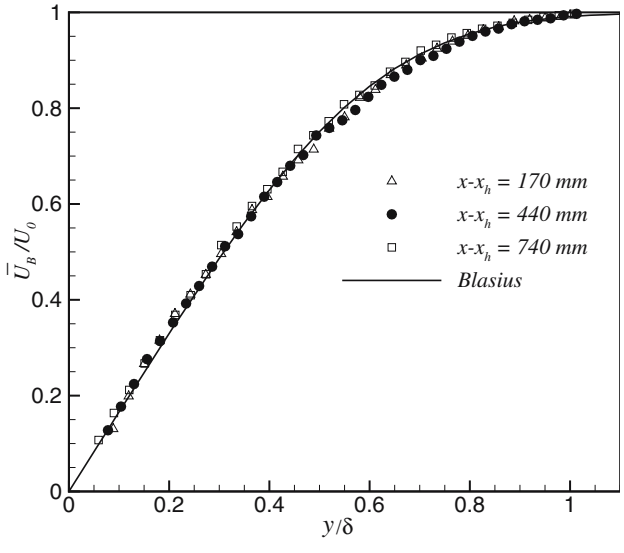

Fig. 3 Laminar base flow compared with the Blasius profile

and 740 mm locations. The hole diameter was the same as that of Amini and Lespinard (1982). Breuer and Haritonidis (1990) used a rectangular membrane that was mounted flush with wall. We will see below that, inspite of the different form of the initial disturbances, the present measurements also capture the early part of the disturbance shape reported by Breuer and Haritonidis (1990).

A constant-temperature hot-wire was used. The single sensing tungsten wire was of 5 μm diameter and was welded to two prongs (length-to-diameter ratio was about 800) of the probe. The overheat ratio was set as 1.5. The hot-wire data were acquired at 2 kHz.

Based on the hot-wire measurement of the fluctuating streamwise velocity component in the freestream, the turbulence level at $x = 0$ was found to be less than 0.05% for the freestream speed of $U_0 \leq 10$ m/s. The streamwise distribution of $C_p = 1 - (U_0/U_R)^2$, in Fig. 2, shows that the streamwise pressure is constant; U_R is the reference freestream velocity at $x = 500$ mm. The measurements reported below were made at a freestream velocity of $U_0 = 4$ m/s.

The PIV unit (M/S IDTpiv, USA) consisted of a double cavity Nd:YAG laser (New Wave Res, 100 mJ), a CCD camera (Sharpvision 1400DE; 1,360×1,036 pixel resolution) and the associated data processing software, proVISION. This data processing software was based on a second-order accurate mesh free algorithm of Lourenco and Krothapalli (2000). In the double exposer mode, the camera could capture five image pairs per second. The flow was seeded by smoke particles (~1 μm; EUROLITE smoke fluid) generated by a commercial fog generator (HP Line), which was placed at about 3,000 mm ahead of the tunnel entry. A laser sheet of around 2 mm thick was used to illuminate the measurement zone; in Fig. 1, this zone in the spanwise plane is depicted by $\Delta x = 47$ mm and $\Delta z = 35$ mm. The thickness of the laser sheet was comparable with the 2 mm thick laser sheet used by Kostas et al. (2002). We may note that at $x - x_h = 11$ mm, the PIV measurements also covered about 8.5 mm upstream of x_h (at which the disturbance was introduced). The same measurement zone was used in the wall normal plane.

A square TTL pulse of 23 ms duration and of 1 Hz frequency was fed to an audio amplifier, which drove the loudspeaker. The loudspeaker was kept outside the tunnel and was connected to the plate by a flexible tube. The same 5 V TTL pulse from the oscillator was fed into the PIV trigger unit to activate both the laser and camera simultaneously. From the hot-wire data at $y/\delta \approx 0.5$, the time (ΔT) taken by the disturbance to travel from the instant of its introduction to a given $x - x_h$ location was measured with respect to a reference TTL pulse; δ is the boundary layer thickness corresponding to $0.99U_0$. The values of ΔT at $x - x_h = 11$, 170, 440, and 740 mm locations were $\Delta T = 46$, 112, 187, and 288 millisecond, respectively. In order to ensure that the propagating disturbance was captured by the PIV, it was phase-locked using a time delay of ΔT, i.e., the TTL pulse triggered both the camera and laser simultaneously after a delay of ΔT.

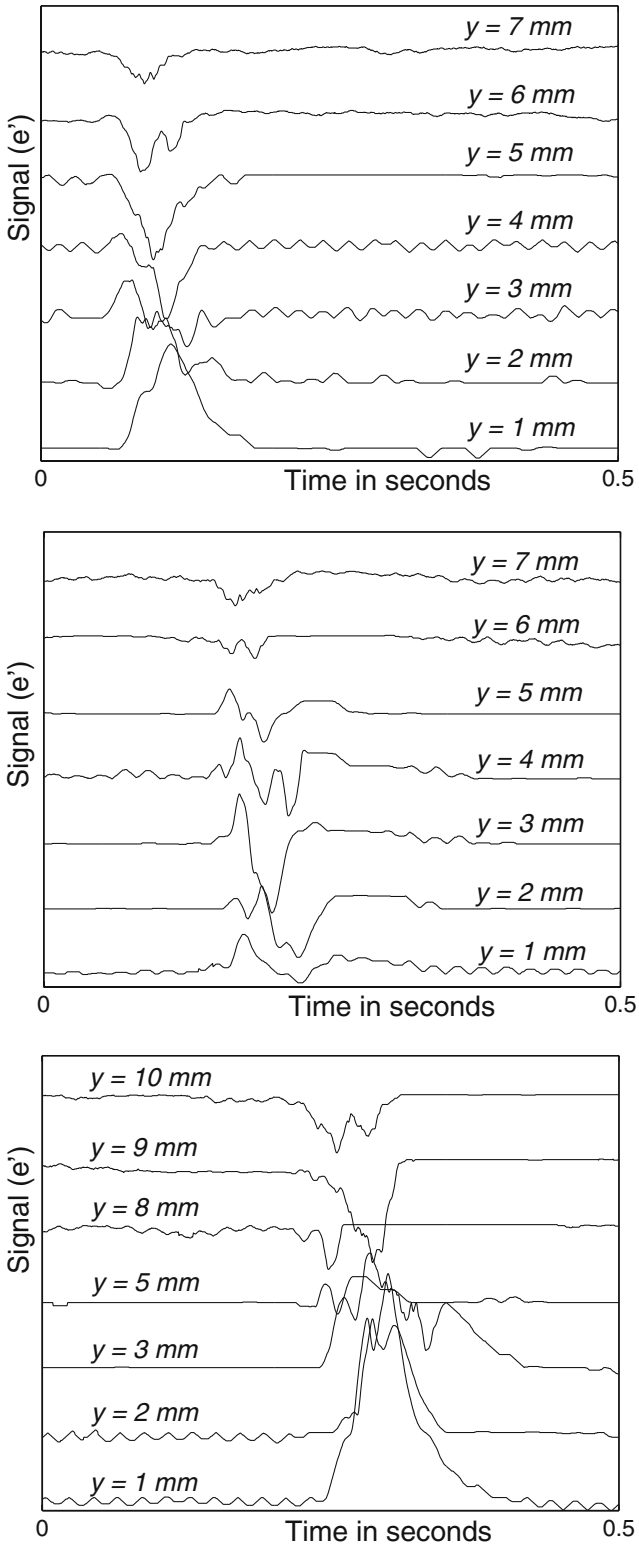

Fig. 4 Twenty ensembles averaged streamwise fluctuating velocity signals at $x - x_h = 170$, 440, and 740 mm locations

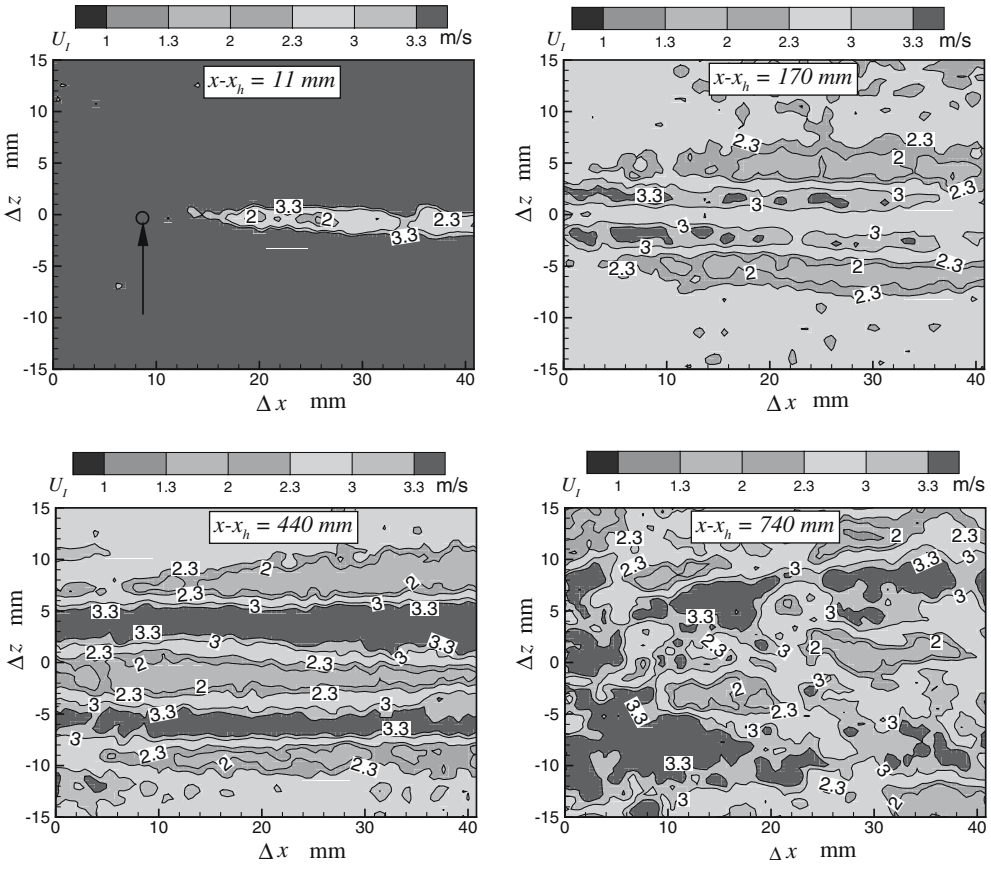

Fig. 5 Contour plots of instantaneous streamwise velocity at $y/\delta \approx 0.5$ by PIV. The *arrow* indicates the position of the hole through which the disturbance was introduced. *Numbers* indicate the contour level of instantaneous streamwise velocity U_I

3 Results and discussions

Initially, hot-wire measurements were made in the laminar boundary layer to establish the Blasius flow and the incipient spot reported by Amini and Lespinard (1982). For the hot-wire measurements, the location of the wall ($y=0$) was determined following Westin et al. (1994). Using a Mitutoyo traverse, the hot-wire was moved vertically at small equidistant points. $y=0$ location was then found by linearly extrapolating the near wall mean velocity data. The streamwise velocity, $\bar{U}_B$, of the undisturbed laminar boundary layer was established as the Blasius at $x - x_h = 170$, 440, 740 mm locations, as shown in Fig. 3. The PIV measurements of the laminar

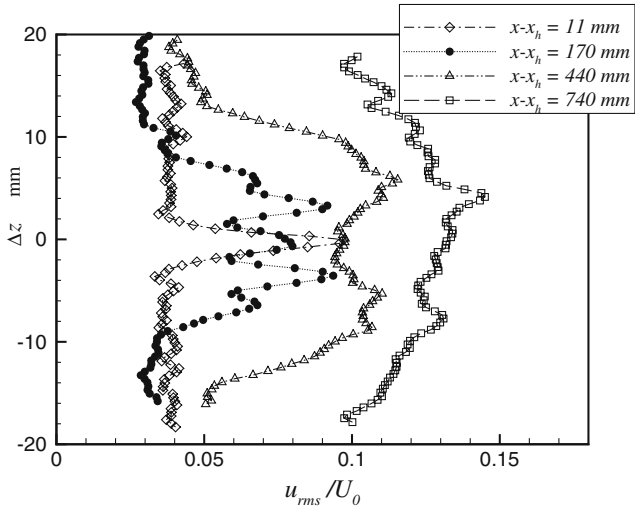

Fig. 6 Spanwise u_{rms} profiles at different downstream locations by PIV

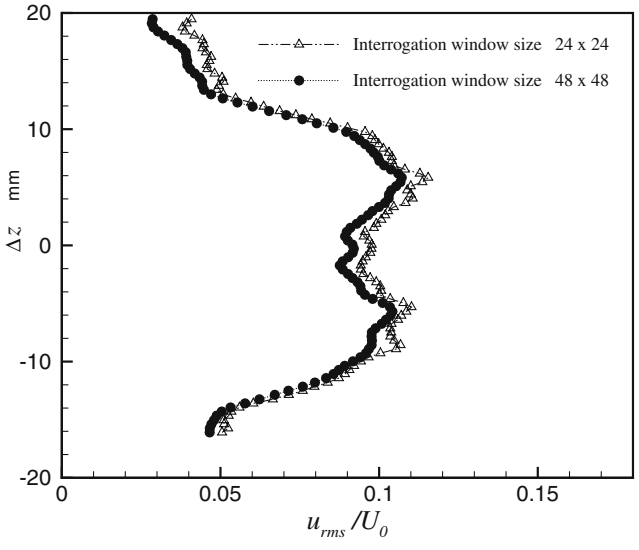

Fig. 7 Spanwise u_{rms} profiles for two different correlation windows at $x - x_h = 440$ mm

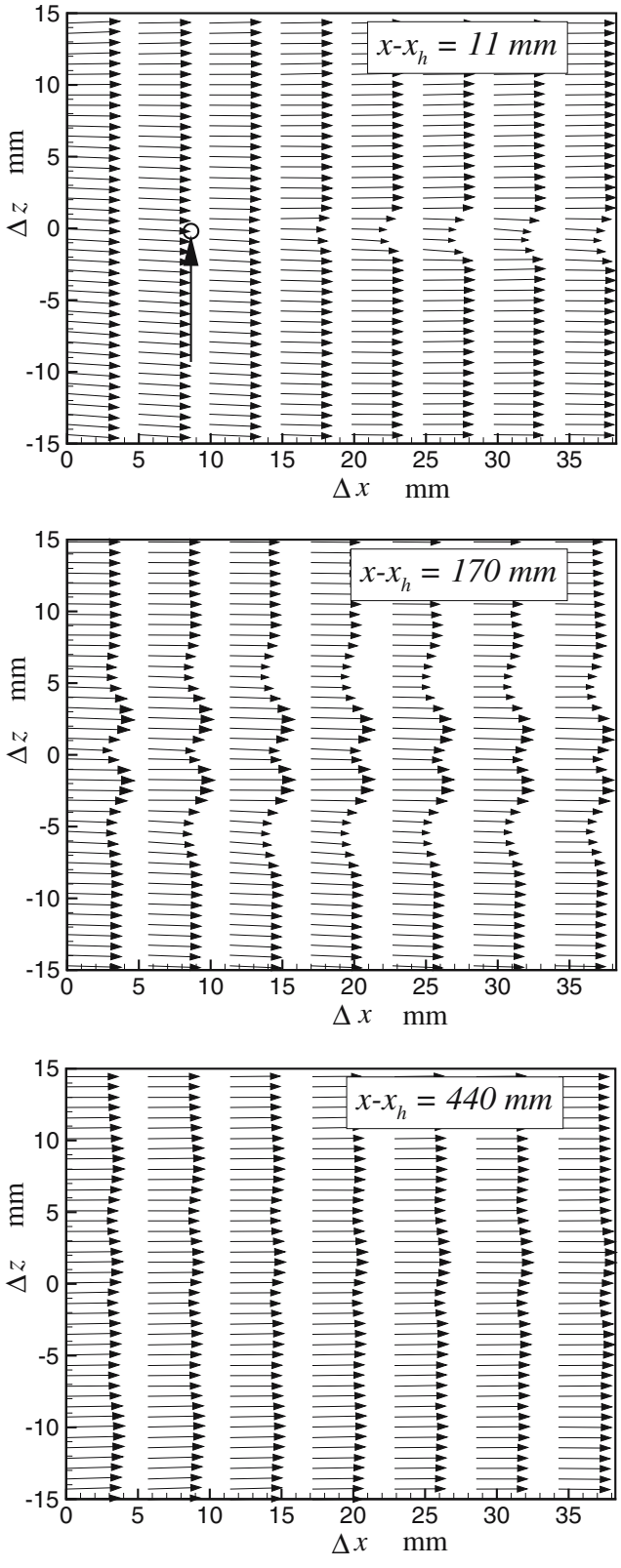

Fig. 8 Mean velocity vectors in the PIV measurement region at three stations. The *vertical arrow* in the *top* frame indicates the location at which the disturbance is introduced. The scale is same in all three frames

boundary layer also reproduced the Blasius boundary layer (Mandal 2005). In the following, δ^*, θ, and $H = \delta^*/\theta$ will denote the displacement thickness, the momentum thickness, and the shape parameter, respectively. The measured values of θ at $x - x_h = 11$, 170, 440, and 740 mm are 0.69, 0.87, 1.08, and 1.29 mm respectively; the corresponding values of R_θ ($= U_0\,\theta/\nu$) are: 178, 224, 276, and 330, respectively. The measured values of $H = 2.58$, 2.58, 2.55, and 2.55 at these stations compare very well with the Blasius value of 2.59.

By adjusting the loudspeaker amplitude from the amplifier, an incipient spot, identified following Amini and Lespinard (1982), was established. The spanwise spread angle was found to be about 12°. The measured

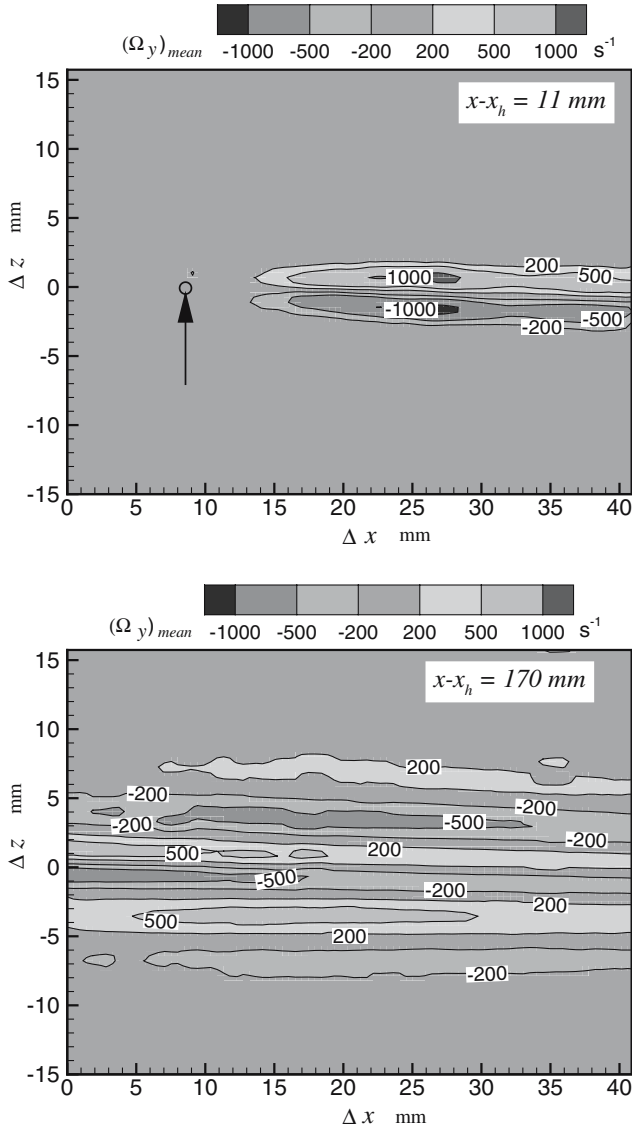

Fig. 9 Mean vorticity in the PIV measurement zone at two stations. The vertical arrow in the top frame indicates the location at which the disturbance is introduced. Numbers indicate the contour level of $(\Omega_y)_{\text{mean}}$

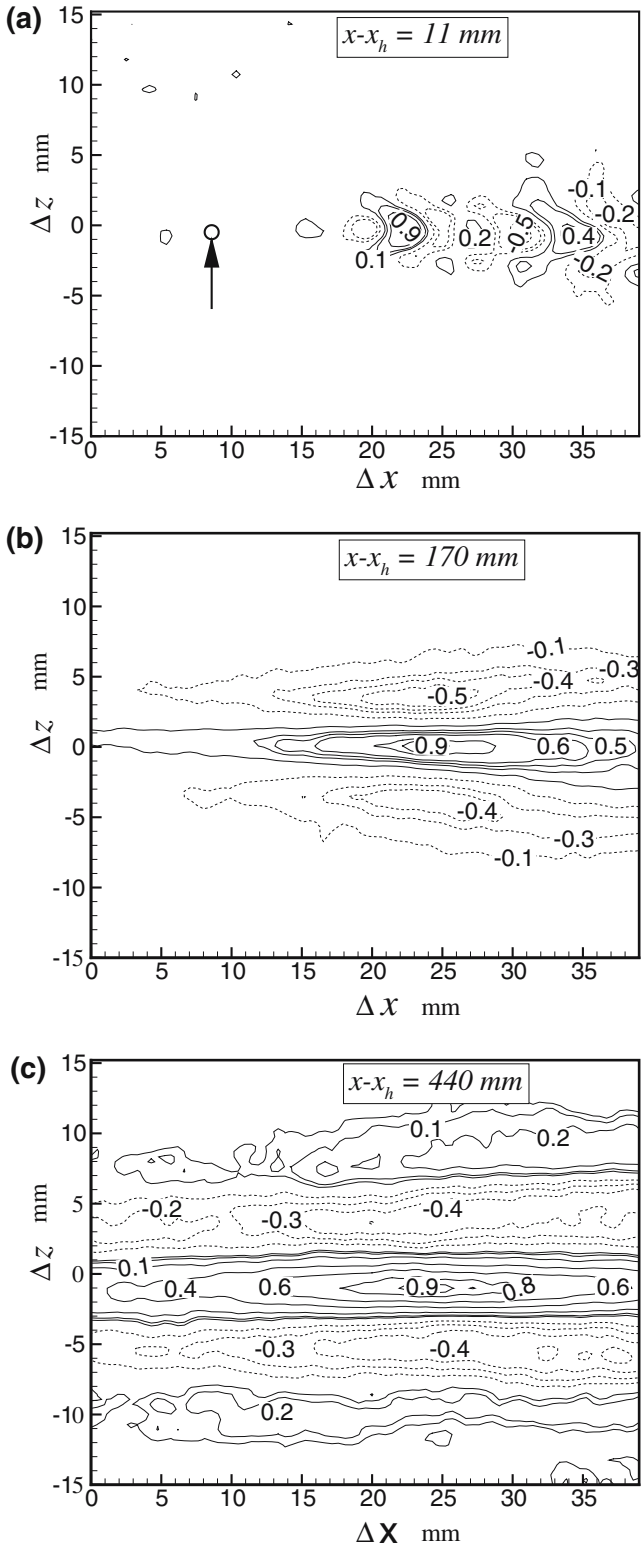

Fig. 10 Contours of R_{uu} from the PIV data in the spanwise plane. The *arrow* in the *top* frame indicates the location at which the disturbance is introduced

hot-wire signals at different y locations in the boundary layer are shown in Fig. 4. It can be seen that these are typical of the incipient spot reported by Amini and Lespinard (1982) in the sense that the disturbance amplitude is spiky away from the wall. As it can be seen in this figure, the flow has become more complex at $x - x_h = 740$ mm. It may be noted that, the critical Reynolds number for the Blasius flow being $(R_\theta)_{\text{crit}} = 200$, as predicted by the linear stability theory, the disturbance introduced was at a sub-critical Reynolds number.

At each measurement station, 400 PIV realizations were acquired. As the PIV processing software, "pro-VISION", was based on a mesh free environment, 100×100 mesh had been used to get 10,000 vectors per frame with 24×24 correlation window. The interpolation limit was five vectors per 10,000 vectors. Hence, the frames which showed more than five vectors interpolation had been skipped. The number of PIV realizations so skipped were about 4–5. That is, the actual number of the PIV realizations considered were 395–396.

For the PIV data, the streamwise instantaneous, the mean, and the fluctuating velocity components are denoted by U_{I}, $\bar{U}$, and $u = U_{\text{I}} - \bar{U}$, respectively. Similarly, in the wall normal direction, V_{I}, $\bar{V}$ and $v = V_{\text{I}} - \bar{V}$ denote the instantaneous, mean and fluctuating velocities, respectively. u_{rms} and v_{rms} are the root-mean-squared values of u and v, respectively. The mean quantities are based on the 395/396 PIV realizations.

3.1 PIV results: spanwise plane

The PIV measurements in the spanwise plane were made at $y/\delta \approx 0.5$. The spanwise distribution of U_I is shown in Fig. 5. The instantaneous frame at $x - x_h = 11$ mm shows that, slightly downstream of the point where the disturbance is introduced (indicated by an arrow), a single streak like structure appears. Further downstream, multiple streaks appear at $x - x_h = 170$ and $x - x_h = 440$ mm, and finally the streaky structure

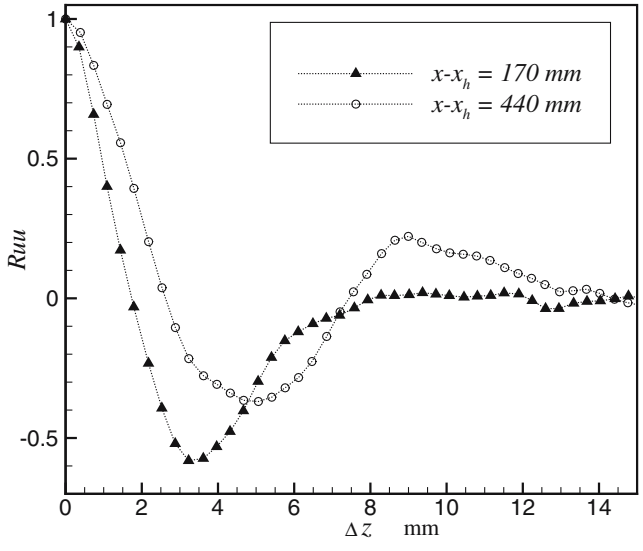

Fig. 11 Plots of the correlation co-efficient in the spanwise direction

appears to have broken down at $x - x_h = 740$ mm. The spanwise variations of u_{rms} at $x - x_h = 11$, 170, 440 and 740 mm locations are shown in Fig. 6. Consistent with the instantaneous picture in Fig. 5, the u_{rms} profiles show that the sharp single peak at $x - x_h = 11$ mm evolves with more peaks in the downstream direction, corresponding to the number of streaks. The difference among the local maxima and minima in the u_{rms} fluctuations are seen to decrease in the downstream direction, and the envelope of the u_{rms} profile has increased considerably in the spanwise direction at $x - x_h = 740$ mm. Since, the disturbance propagates within a spanwise envelope of 12° included angle, the non-zero values of u_{rms}/U_0 outside this zone is attributed to the PIV noise. As Christensen (2004) points out, the PIV measurements are not free from the random and bias errors. He further suggests that the random error can be reduced by taking an average of large ensemble. With this in mind, the mean values from the PIV data reported here are based on the entire 395/396 PIV realizations, as mentioned earlier. The interrogation window size is also important (Foucaut et al. 2004). As an example, we have considered a 48×48 pixels interrogation window for the data at $x - x_h = 440$ mm. Compared

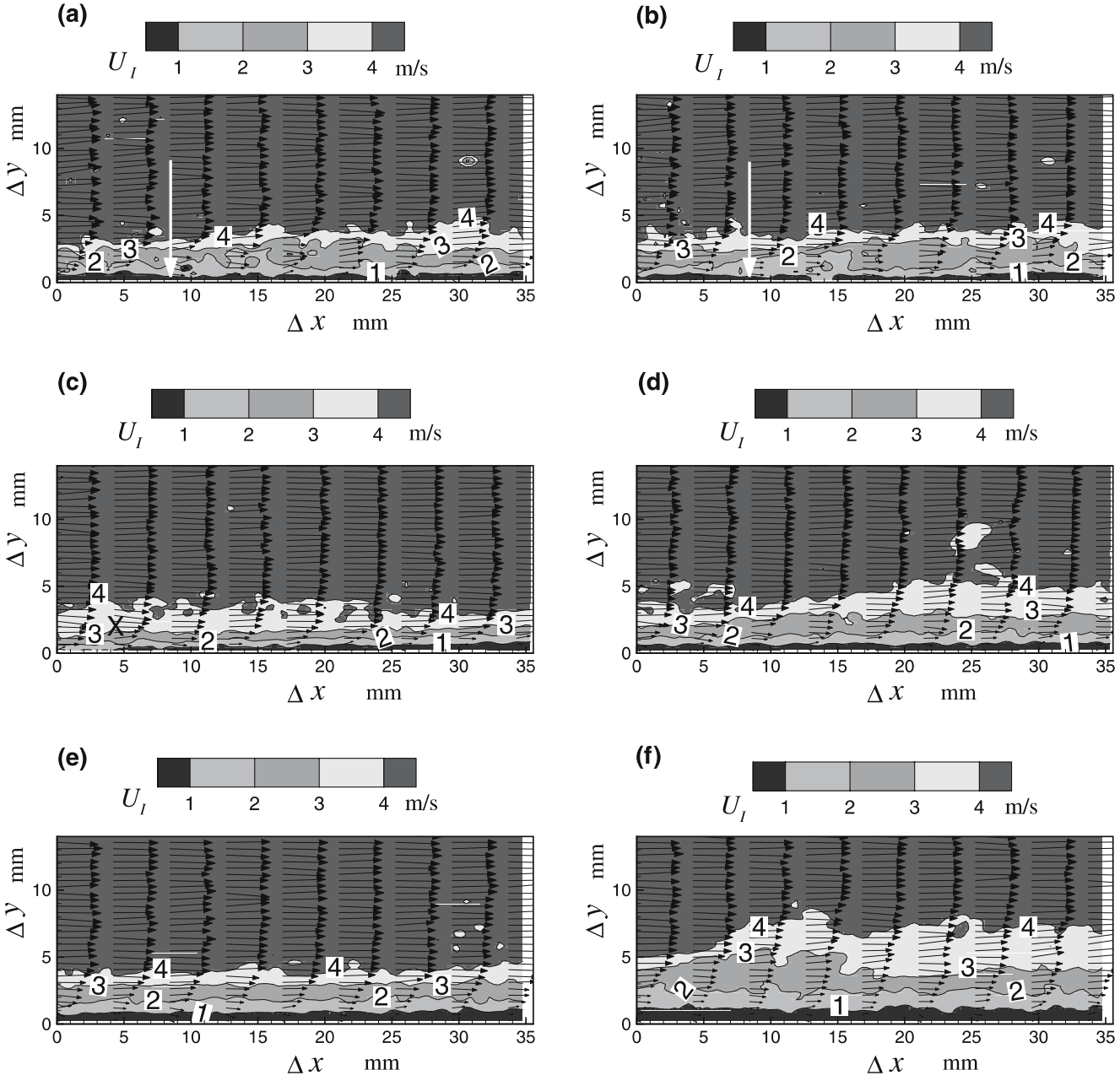

Fig. 12 Instantaneous velocity vectors in the background of instantaneous streamwise velocity. **a**, **b** $x - x_h = 17$ mm; **c**, **d** $x - x_h = 170$ mm; **e**, **f** $x - x_h = 440$ mm. The *vertical arrow* indicates the position at which the disturbance was introduced. *Numbers* indicate the contour level of the instantaneous streamwise velocity U_I

to 24×24 pixels window, the u_{rms}/U_0 data show a slight reduction for -8 mm $\leq \Delta z \leq 8$ mm and beyond $\Delta z = \pm 14$ mm, as shown in Fig. 7. However, a larger window size leads to a bad signal-to-noise ratio (Foucaut et al. 2004). We may note that, except for comparison, we have not used 48×48 pixels interrogation window. Apart from the PIV noise, the propagating disturbance may create instability outside its propagation cone, as in the case of a turbulent spot where the Tollmien-Schlichting waves are seen near the wing tips (Wygnanski et al. 1979).

Since we are interested in the evolution of the incipient spot prior to its breakdown, we consider the results at $x - x_h = 11$, 170, and 440 mm locations only, in the following.

The spanwise variation of $\bar{U}$ at different stations are shown in term of the velocity vectors in Fig. 8. The vertical arrow in the top frame for $x - x_h = 11$ mm indicates the point at which the disturbance was introduced. Only a single velocity deficit is seen in the early stage at $x - x_h = 11$ mm. It can be verified that the spread angle is about 12°. The velocity deficit seems to show up at $\Delta x \sim 15$ mm. Since these measurements are at $y/\delta \approx 0.5$, the effect of the disturbance introduced at x_h is not felt at this boundary layer location till at $\Delta x \sim 15$ mm. Downstream, the flow develops a wavy pattern at $x - x_h = 170$ mm that persists further downstream at $x - x_h = 440$ mm, but at a reduced amplitude. Effectively, this spanwise variation of $\bar{U}$ implies the presence of low and high speed streaks. Although, Amini and Lespinard (1982) also observed similar waviness, their hot-wire measurements do not report the early development like the one reported here at $x - x_h = 11$ mm, nor any streak like structure over such a large spatial extent. The wavy structure seen here is similar to the the pattern in the x–t plane reported by Breuer and Haritonidis (1990). The mean Ω_y vorticity is shown in Fig. 9. Both positive and negative Ω_y appear in pair about $\Delta z = 0$ (which corresponds to $z = 0$). Also, the number of vorticity streaks increase in the downstream direction. In studying turbulent spot, Schröder and Kompenhans (2004) mention that the presence of positive and negative vorticity streaks inside the spot may cause the center-line symmetry. The positive and negative vorticity streaks in Fig. 9 thus suggest the observed symmetry of the propagating disturbance.

In order to find the coherent structure, the two-point spatial correlation, R_{uu}, of the fluctuating streamwise velocity component u is estimated:

$$R_{uu}(x_0, z_0, \mathrm{d}x, \mathrm{d}z) = \frac{\overline{u(x_0, z_0, t)u(x_0 + \mathrm{d}x, z_0 + \mathrm{d}z, t)}}{\sqrt{\overline{u^2(x_0, z_0)}}\sqrt{\overline{u^2(x_0, z_0)}}}$$

where (x_0, z_0) is the reference point. The correlation contours at $x - x_h = 11$, 170, and 440 mm are shown in Fig. 10. This figure also confirms the downstream development of the streaky pattern. The iso-contours at $x - x_h = 11$ mm show a remarkable similarity with that of Breuer and Haritonidis (1990), inspite of the fact that their initial disturbance is different from that used in the present study. These authors have reported the disturbance shape in a frozen time scale in the sense

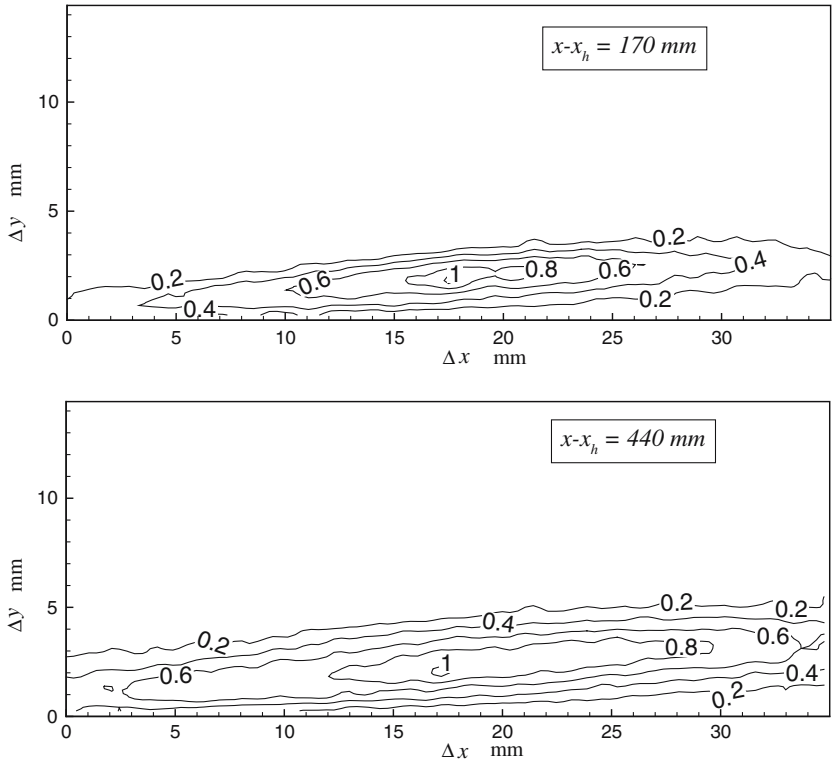

Fig. 13 Contours of R_{uu} in the wall normal plane at two stations

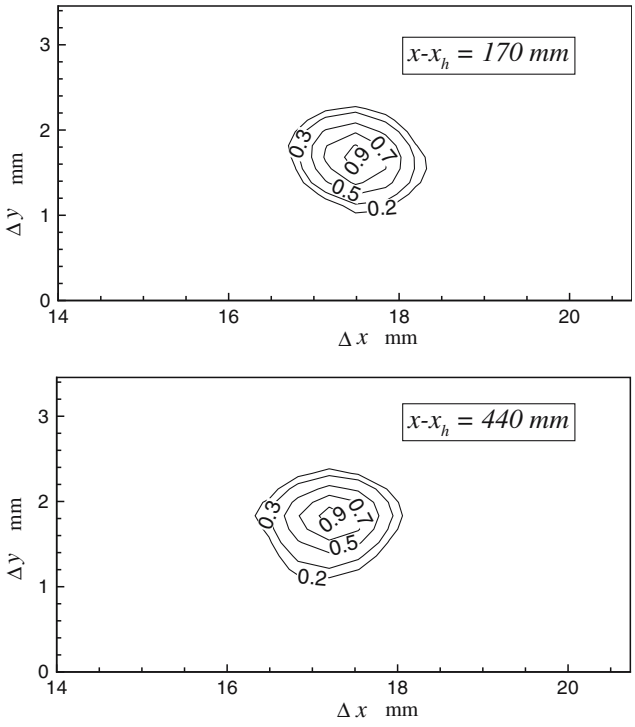

Fig. 14 Spatial correlation contours of the fluctuating wall normal velocity component at two stations

that the downstream shape does not change considerably. Compared to this, the long streaky structures at $x - x_h = 170$ and 440 mm locations (Fig. 10) are different. These streaks are similar to those reported by other investigators with different disturbance sources, introduced either in the freestream or at the wall (see Boiko et al. 2002). The streamwise periodicity of the disturbance seen at $x - x_h = 11$ mm in Fig. 10 is attributed to the following fact. The loudspeaker during its upstroke pushes fluid away from the wall, and sucks fluid during its downstroke. These events cause both low and high speed regions, whose signature exhibits the periodic feature in the early stage at $x - x_h = 11$ mm. The streak spacing has been calculated from Fig. 11, which shows the variation of R_{uu} with Δz. The distance between the origin and the point of the minimum value of R_{uu} in Fig. 11 can be interpreted as half the dominating spanwise wavelength of high and low speed streaks. It is found that the streak spacing ranges from 0.8δ to 1δ and does not scale with the boundary layer thickness, as reported by Bakchinov et al. (1994), who have observed streaks for puff introduced upstream of the plate leading edge, as in the experiment of Westin et al. (1998).

3.2 PIV results: wall normal plane along z = 0

Due to the difficulty in placing the camera in the $x - y$ plane at $x - x_h = 11$ mm, the measurements were made at $x - x_h = 17$ mm downstream of x_h, i.e., about 6 mm downstream of the measurement station at $x - x_h = 11$ mm. The PIV measurements in the wall normal plane have revealed that the boundary layer oscillates. The oscillation, however, is small at $x - x_h = 17$ mm. Some representative instantaneous PIV frames at $x - x_h = 17$, 170 and 440 mm depict this aspect in Fig. 12. The vertical arrows in Fig. 12a and b

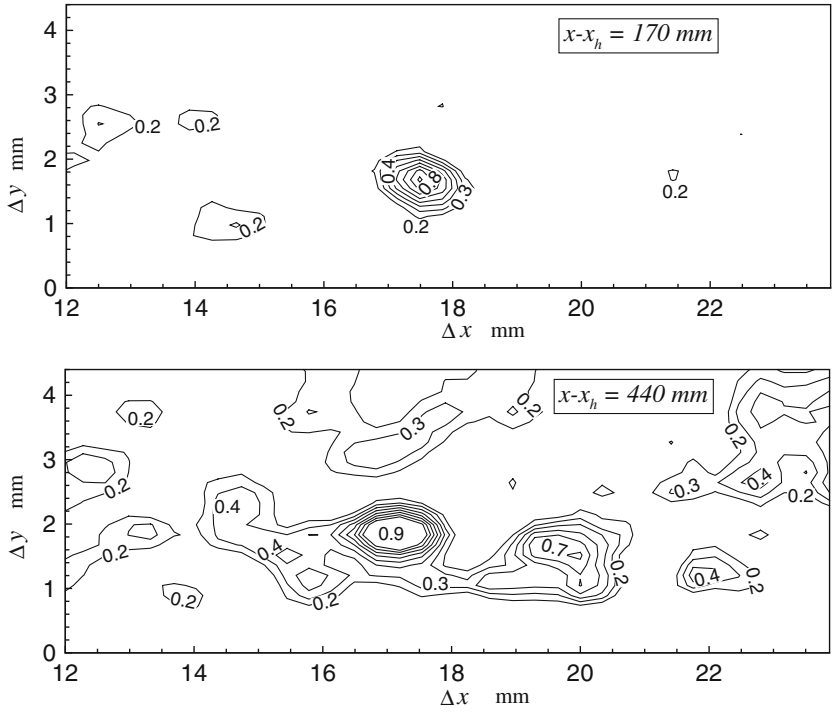

Fig. 15 Correlation contours of the Reynolds stress in the wall normal plane at two stations

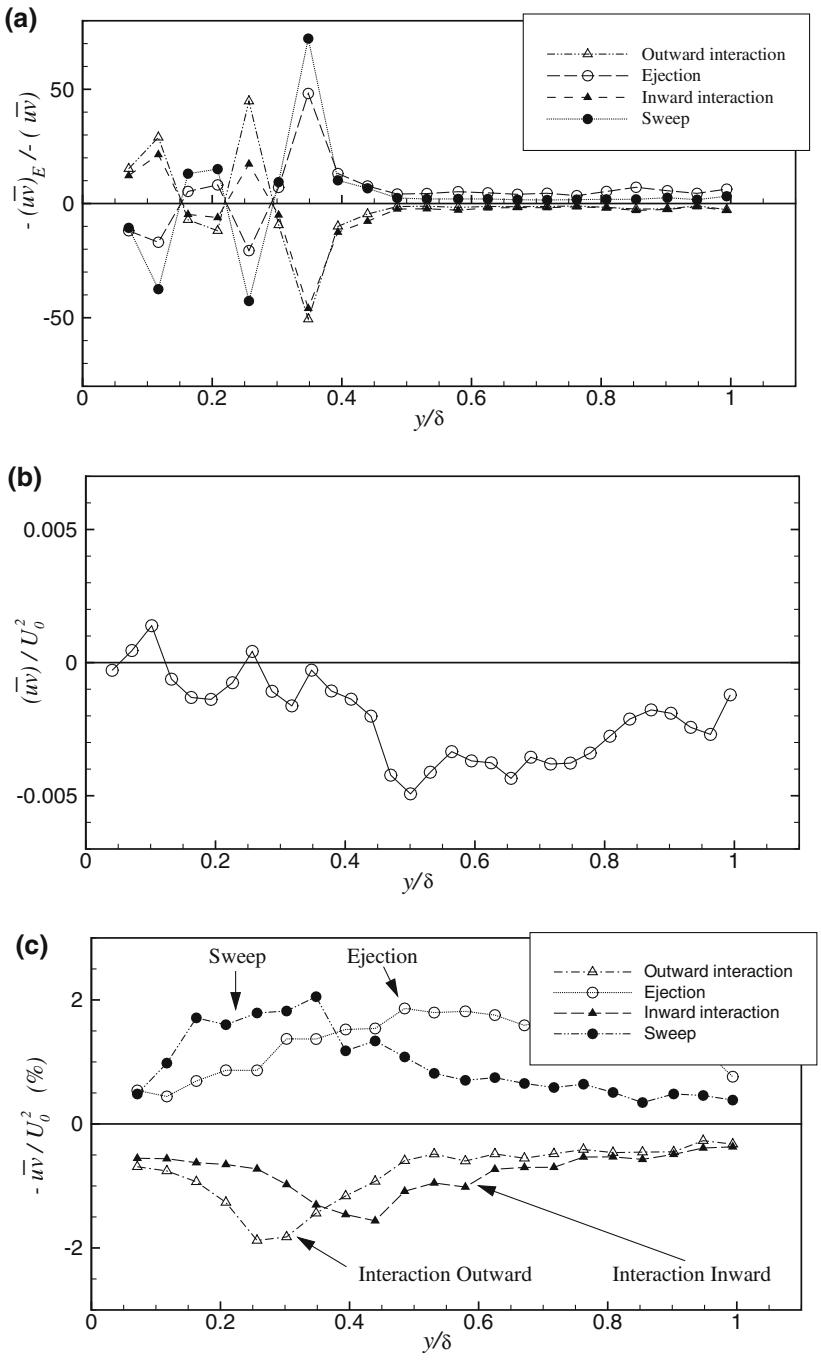

Fig. 16 Various Reynolds stress events (**a**, **c**) and the Reynolds stress variation (**b**) in the boundary layer. The measurement location is $x - x_h = 440$ mm

indicate the location at which the disturbance was introduced. Compared to the PIV frames at $x - x_h = 17$ mm (Fig. 12a, b), the oscillation of the boundary layer is more pronounced in Fig. 12e and f, for $x - x_h = 440$ mm location. While similar boundary layer oscillations are also seen in the simulation of the bypass transition by Jacobs and Durbin (2001), the oscillation of the boundary layer in the presence of an incipient spot is not yet reported in the available literature, or has been ignored. These oscillations are possibly due to the spanwise modulation of the streaky structures in the boundary layer.

Using the measured $\bar{U}$ (from 395/396 PIV realizations), θ and δ^* were estimated. The measured values of $H = \delta^*/\theta$ at $x - x_h = 170$ and 440 mm were 2.04 and 2.10, respectively. The reduced value of H, compared to the Blasius value of 2.59, indicates the presence of streamwise pressure gradient. However, the freestream velocity being constant at 4 m/s, this reduction in H is attributed to the generation of the Reynolds stress (Westin et al. 1994), as also confirmed from the downstream growth of u_{rms}/U_0 seen in Fig. 6.

In the wall normal plane, the spatial correlations of u, v, and the Reynolds stress have been estimated:

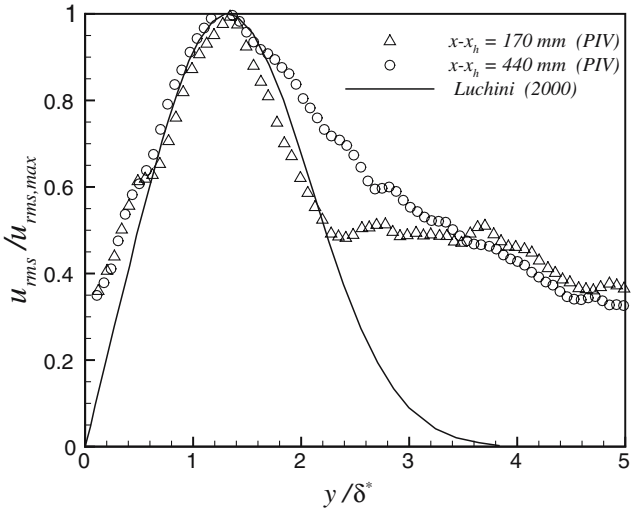

Fig. 17 Variation of $u_{\rm rms}/u_{\rm rms}$ with y/δ^* compared with Luchini's theory

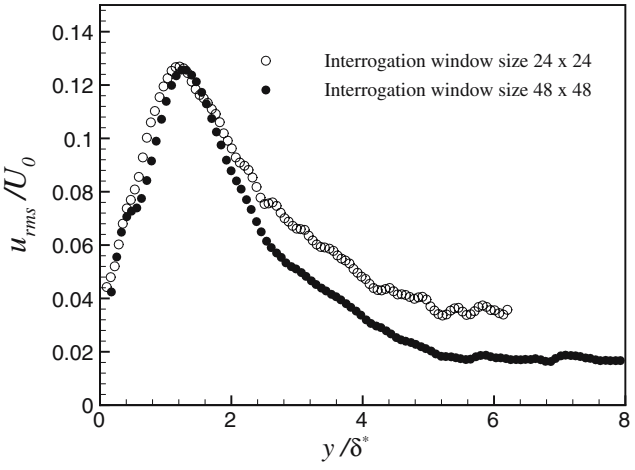

Fig. 18 Wall normal $u_{\rm rms}$ profiles at $x - x_h = 440$ mm location for two different correlation windows

$$R_{uu}(x_0, y_0, \mathrm{d}x, \mathrm{d}y) = \frac{\overline{u(x_0, y_0, t)u(x_0 + \mathrm{d}x, y_0 + \mathrm{d}y, t)}}{\sqrt{\overline{u^2(x_0, y_0)}}\sqrt{\overline{u^2(x_0, y_0)}}}$$

$$R_{vv}(x_0, y_0, \mathrm{d}x, \mathrm{d}y) = \frac{\overline{v(x_0, y_0, t)v(x_0 + \mathrm{d}x, y_0 + \mathrm{d}y, t)}}{\sqrt{\overline{v^2(x_0, y_0)}}\sqrt{\overline{v^2(x_0, y_0)}}}$$

$$R_{uv,uv}(x_0, y_0, \mathrm{d}x, \mathrm{d}y) = \frac{\overline{uv(x_0, y_0, t)uv(x_0 + \mathrm{d}x, y_0 + \mathrm{d}y, t)}}{\overline{u^2(x_0, y_0)v^2(x_0, y_0)}}$$

where (x_0, y_0) is the reference point. The contours of R_{uu} in Fig. 13 show an inclined and stretched structures; for clarity the contour levels are shown for $R_{uu} \geq 0.2$. In the downstream direction, the flow has undergone a noticeable stretching and thickening at $x - x_h = 440$ mm. The R_{vv} contours, on the other hand, has a frozen and coherent structure, as shown in Fig. 14; for clarity the contour levels are shown for $R_{vv} \geq 0.2$. We may note that the peak value of $v_{\rm rms}$ is found to be about 30% of the peak value of $u_{\rm rms}$. This suggests that the streamwise fluctuation is more dominant. The frozen R_{vv} contours (in Fig. 14) possibly imply that the propagating disturbance does not cause a significant Reynolds stress production. The $R_{uv,uv}$ contours in Fig. 15 show a frozen structure in the same region as in the case of R_{vv} (in Fig. 14). In addition, downstream of this frozen region, highly correlated $R_{uv,uv}$ contours appear in the region 19mm $\leq \Delta x \leq$ 20.5 mm at $x - x_h = 440$ mm. In turbulent flows, the quadrant analysis of the fluctuating velocity components provide an insight into the Reynolds stress production via the ejection and sweep events. In turbulent spots, the quadrant analysis by Schröder and Kompenhans (2004) has revealed important flow structures involving the ejection and sweep events. Following Wallace et al. (1972), we have carried out the quadrant analysis at $x - x_h = 440$ mm; in terms of Δx (see Fig. 1), the PIV data are at $\Delta x/2$. The mean boundary layer thickness at this location is $\delta = 10.3$ mm. Various events are defined as: ejection, $u < 0$, $v > 0$; sweep, $u > 0$, $v < 0$; outward interaction, $u > 0$, $v > 0$; inward interaction, $u < 0$, $v < 0$. For these events, the average of the PIV realizations of the quantity uv is denoted by $\overline{(uv)}_E$. Various events thus identified are shown in Fig. 16a; as in Wallace et al. (1972), $-\overline{(uv)}_E$ is normalized by $-\overline{uv}$. Since the measured $-\overline{uv}/U_0^2$ in the boundary layer is found to fluctuate till $y/\delta \approx 0.35$, as shown in Fig. 16b, the interpretation of the events in Fig. 16a becomes difficult, except that various events seen in turbulent flows are also seen here. For instance, the sweep event is more than the ejection event for $0.15 \leq y/\delta \leq 0.25$ and $0.3 \leq y/\delta \leq 0.4$ in Fig. 16a. One important result in Fig. 16b is that the Reynolds stress is maximum at $y/\delta \approx 0.5$, i.e., it is away from the wall. When $\overline{(uv)}_E$ is normalized by $U^2{}_0$, various events displayed in Fig. 16c show similarity with those observed by Wallace et al. (1972) in turbulent flows. For example, the sweep event is more important for $y/\delta \leq 0.35$ and the ejection event becomes dominant thereafter. The interacting events in Fig. 16c are also similar to those of Wallace et al. (1972). However, the meaning of the quantity $-\overline{(uv)}_E/U_0^2$ is not the same as that of $-\overline{(uv)}_E/-\overline{uv}$. Also, since our measurements are only along $z = 0$, we cannot infer the flow topology in terms of the ejection and sweep events, as carried out by Schröder and Kompenhans (2004) in turbulent spots using multi-plane stereo PIV. (These analyses follow from the suggestion of an anonymous referee, and we thank him.)

The streaky structures of low and high speed fluids seen in the spanwise plane in Fig. 5 resembles those in bypass transition (Jacobs and Durbin 2001; Matsubara and Alfredsson 2001). Luchini (2000) has proposed that $u_{\rm rms}/u_{\rm rms,\ max}$ has a self-similar structure when plotted against y/δ^*. Independently, Andersson et al. (1999)

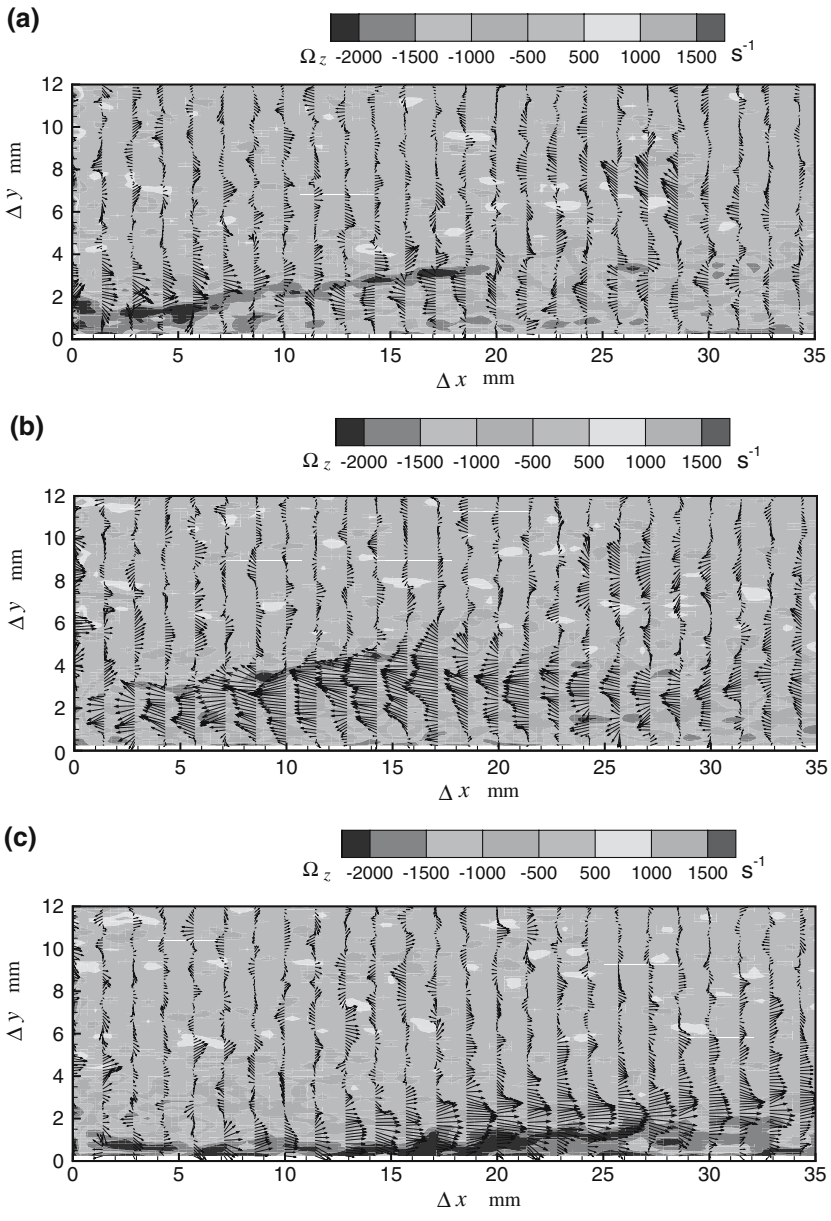

Fig. 19 Three instantaneous PIV frames of fluctuating velocity vectors in the background of instantaneous vorticity at $x - x_h = 170$ mm location. *Darker region* within boundary layer indicates high negative instantaneous vorticity Ω_z

have proposed the same self-similar feature. The measured $u_{\mathrm{rms}}/u_{\mathrm{rms,\ max}}$ profiles at $x - x_h = 170$ and 440 mm are compared with the theory of Luchini (2000) in Fig. 17. It can be seen that some self-similarity feature is present over a large portion of the boundary layer. The difference, however, is expected in view of the fact that

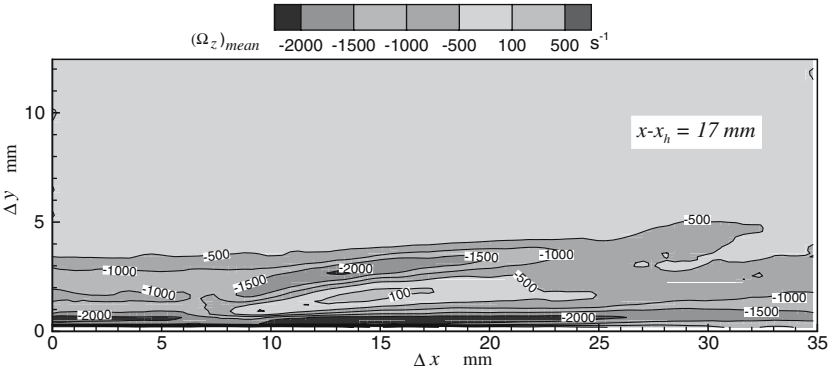

Fig. 20 Mean vorticity of entire PIV realizations at $x - x_h = 17$ mm location in the wall normal plane. Lifted high shear layer in $8.5 \leq \Delta x \leq 20$. *Numbers* indicate the contour level of $(\Omega_z)_{\mathrm{mean}}$

streaks develop near the leading edge in bypass transition, compared to the present study. One can see in this figure that $u_{rms}/u_{rms,\ max}$ is non-zero outside the boundary layer. This non-zero value may in part be attributed to the PIV noise. Also, although a black sticker was used to reduce the reflection of the laser sheet, the reflection was not completely eliminated. Thus, a part of the noise could be due to this reflection in the wall normal plane. We also find that a larger interrogation window of 48×48 pixels reduces this noise without affecting the values within the boundary layer, as shown in Fig. 18 for $x - x_h = 440$ mm, as an example. Jacobs and Durbin's (2001) DNS results of bypass transition clearly show the presence of spanwise low and high speed streaks and both 'backward' and 'forward' jets of the fluctuating velocity components (u and v). Similar jet-like structures are also observed by us at $x - x_h = 170$ and 440 mm, where streaks are quite developed. As an example, three instantaneous frames depicting such jet-like structures at $x - x_h = 170$ mm are shown in Fig. 19, where the fluctuating velocity vectors are displayed in the background of the instantaneous Ω_z vorticity (darker region). One observes in this figure some concentrated positive and negative fluctuations. Similar fluctuations are also seen in the experimental study of bypass transition (Mandal 2005). Figure 19a and b also show some high intensity fluctuations in the freestream in the region 6 mm $\leq \Delta y \leq$ 9 mm and 25 mm $\leq \Delta x \leq$ 26.5 mm; the value of δ at this station is 9.2 mm. A frame by frame analysis of the PIV realizations has revealed that, occasionally the flow near the boundary layer edge gets detached from the tip of the inclined shear layer. This detached flow appears as fluctuations in the freestream. Mean Ω_z vorticity at $x - x_h = 17$ mm is shown in Fig. 20. A tilted high shear region can be seen. Since, the development of streaks is associated with the lift-up effect (Boiko et al. 2002), the lift-up of high shear layer in Fig. 20 is expected, as also suggested by Breuer and Haritonidis (1990).

4 Conclusions

The PIV technique has been used to study the spatial evolution of an incipient spot triggered by a small amplitude disturbance that is introduced into a constant pressure boundary layer. Well defined high and low speed streaks are observed in the spanwise plane. Compared to the hot-wire measurements, the PIV measurements have enabled to observe these streaks over large spanwise and streamwise extent without invoking the propagation velocity of the spot. From the spatial correlations of the fluctuating velocity components in the wall normal plane we conclude that the structure of the streamwise component is stretched one, but that of the wall normal component is frozen in space. An incipient spot is found to cause the boundary layer oscillation and the 'forward' and 'backward' jet-like structures of the fluctuating velocity components; these results are not yet reported in the available literature. These jet-like structures are similar to those seen in the simulation of the bypass transition. On the whole, an incipient spot bears some features of the bypass transition.

Acknowledgments The authors sincerely thank the Department of Science and Technology for funding the PIV unit through the FIST programme.

References

Amini J, Lespinard G (1982) Experimental study of an "incipient spot" in a transitional boundary layer. Phys Fluids 25:1743–1750

Andersson P, Berggren M, Henningson DS (1999) Optimal disturbances and bypass transition in boundary layers. Phys Fluids 11:134–150

Bakchinov AA, Westin KJA, Kozlov VV, Alfredsson PH (1994) On the receptivity of a flat plate boundary layer to localized free stream disturbances. In: IUTAM Symposium, Sendai, pp 341–348

Boiko AV, Grek GR, Dovgal AV, Kozlov VV (2002) The origin of turbulence in near-wall flows. Springer, Berlin Heidelberg New York

Breuer KS, Haritonidis JH (1990) The evolution of a localized disturbance in a laminar boundary layer. Part 1. Weak disturbances. J Fluid Mech 220:569–594

Christensen KT (2004) The influence of peak-locking errors on turbulence statistics computed from PIV ensembles. Exp Fluids 36:484–497

Foucaut JM, Carlier J, Stanislas M (2004) PIV optimization for the study of turbulent flow using spectral analysis. Meas Sci Technol 15:1046–1058

Gaster M, Grant I (1975) An experimental investigation of the formation and development of a wave packet in a laminar boundary layer. Proc R Soc Lond A 347:253–269

Gutmark E, Blackwelder RF (1987) On the structure of turbulent spot in a heated laminar boundary layer. Exp Fluids 5:217–229

Jacobs RG, Durbin PA (2001) Simulations of bypass transition. J Fluid Mech 428:185–212

Kostas J, Soria J, Chong MS (2002) Particle image velocimetry measurements of a backward-facing step flow. Exp Fluids 33:838–853

Lourenco LM, Krothapalli A (2000) TRUE resolution PIV: a mesh-free second order accurate algorithm. In: Proceedings of the International Conference in applications of lasers to fluid mechanics, Lisbon

Luchini P (2000) Reynolds number independent instability of the boundary-layer over a flat surface: optimal perturbations. J Fluid Mech 404:289–309

Mandal AC (2005) Particle image velocimetry (PIV) measurements in a low intermittency transitional flow. Master of Science Thesis, Department of Aerospace Engineering, Indian Institute of Science

Matsubara M, Alfredsson PH (2001) Disturbance growth in boundary layers subjected to free-stream turbulence. J Fluid Mech 430:149–168

Narasimha R, Prasad SN (1994) Leading edge shape for flat plate boundary layer studies. Exp Fluids 17:358–360

Narasimha R, Devasia KJ, Gururani G, Badri Narayanan MA (1984) Transitional intermittency in boundary layers subjected to pressure gradient. Exp Fluids 2:171–176

Schröder A, Kompenhans J (2004) Investigation of a turbulent spot using multi-plane stereo particle image velocimetry. Exp Fluids 36:82–90

Schubauer GB, Klebanoff PS (1955) Contribution on the mechanics of boundary layer transition. NACA TN-3489

Vasudevan KP, Dey J, Prabhu A (2001) Spot propagation characteristics in laterally strained boundary layers. Exp Fluids 30:488–491

Wallace JM, Eckelmann H, Brodkey RS (1972) The wall region in turbulent shear flow. J Fluid Mech 54:39–48

Westin KJA, Boiko AV, Klingmann BGB, Kozlov VV, Alfredsson PH (1994) Experiments in a boundary layer subjected to free stream turbulence. Part 1. Boundary layer structure and receptivity. J Fluid Mech 281:193–218

Westin KJA, Bakchinov AA, Kozlov VV, Alfredsson PH (1998) Expereiments on localized disturbances in a flat plate boundary layer. Part 1. The receptivity and evolution of a localized free stream disturbance. Eur J Mech B/Fluids 17:823–846

Wygnanski I, Haritonidis JH, Kaplan RE (1979) On Tollmien-Schlichting wave packet produced by a turbulent spot. J Fluid Mech 92:505–528

Wygnanski I, Zilberman M, Haritonidis JH (1982) On the spreading of turbulent spot in the absence of a pressure gradient. J Fluid Mech 123:69–90